Published in final edited form as:
Cancer Cell. 2014 December 8; 26(6): 909–922. doi:10.1016/j.ccell.2014.10.019.

Targeting Transcriptional Addictions In Small Cell Lung Cancer With a Covalent CDK7 Inhibitor

Camilla L. Christensen[1], **Nicholas Kwiatkowski**[2], **Brian J. Abraham**[2], **Julian Carretero**[3], **Fatima Al-shahrour**[4], **Tinghu Zhang**[5], **Edmond Chipumuro**[6], **Grit S. Herter-Sprie**[1], **Esra A. Akbay**[1], **Abigail Altabef**[1], **Jianming Zhang**[5], **Takeshi Shimamura**[7], **Marzia Capelletti**[1], **Jakob B. Reibel**[1], **Jillian Cavanaugh**[1], **Peng Gao**[1], **Yan Liu**[1], **Signe R. Michaelsen**[8], **Hans S. Poulsen**[8], **Amir R. Aref**[1], **David A. Barbie**[1], **James E. Bradner**[1], **Rani George**[6], **Nathanael S. Gray**[5,10], **Richard A. Young**[2,10], and **Kwok-Kin Wong**[1,9,10]

[1]Department of Medical Oncology, Dana-Farber Cancer Institute, Harvard Medical School, Boston 02215, MA, USA

[2]Whitehead Institute for Biomedical Research, Massachusetts Institute of Technology, Cambridge 02142, MA, USA

[3]Departament de Fisiologia, Facultat de Farmacia, Universitat de Valencia, Valencia 46010, Spain

[4]Translational Bioinformatics Unit, Clinical Research Programme, Spanish National Cancer Research Centre, Madrid 28029, Spain

[5]Department of Cancer Biology, Dana-Farber Cancer Institute, Boston 02215, MA, USA

[6]Department of Pediatric Hematology/Oncology, Dana-Farber Cancer Institute and Children's Hospital, Boston 02215, MA, USA

[7]Department of Molecular Pharmacology and Therapeutics, Oncology Research Institute, Loyola University Chicago, Stritch School of Medicine, Maywood 60153, IL, USA

Corresponding authors: Kwok-Kin Wong, Department of Medical Oncology, Dana-Farber Cancer Institute, 450 Brookline Avenue, Boston, MA, 02215-5450, USA, Phone: 617-632-6084; Fax: 617-582-7683; kwong1@partners.org. Richard A. Young, Whitehead Institute for Biomedical Research, 9 Cambridge Center, Cambridge, MA 02142, Phone: 617-258-5219, Fax: 617-258-5218; young@wi.mit.edu.
[10]Co-senior authors

CONFLICT OF INTEREST

Richard A. Young, Nathanael S. Gray and James E. Bradner are founders and equity holders in Syros that has licensed the CDK7 intellectual property from DFCI. Nicholas Kwiatkowski, Tinghu Zhang and Nathanael S. Gray are inventors on a patent application covering THZ1.

Accession number

GEO accession number for the microarray and ChIP-seq data reported in this paper is GSE62614.
Cellular viability, proliferation and apoptosis; 3D matrix *in vitro* assay; Western Blotting; Bio-THZ1 pulldown, cDNA synthesis and quantitative PCR; Immunohistochemistry; Xenograft dosing studies; Gene Set Enrichment Analysis; Functional gene ontology (GO) analysis. A full description of these methods is listed in Supplemental Experimental Procedures.

[8]Department of Radiation Biology, The Finsen Center, Copenhagen University Hospital, Copenhagen 2100, Denmark

[9]Belfer Institute for Applied Cancer Science, Dana-Farber Cancer Institute, Boston 02215, MA, USA

SUMMARY

Small cell lung cancer (SCLC) is an aggressive disease with high mortality. The identification of effective pharmacological strategies to target SCLC biology represents an urgent need. Using a high-throughput cellular screen of a diverse chemical library we observe that SCLC is sensitive to transcription-targeting drugs, and in particular to THZ1, a recent identified covalent inhibitor of cyclin-dependent kinase 7 (CDK7). We find that expression of super-enhancer associated transcription factor genes including *MYC* family proto-oncogenes and neuroendocrine lineage-specific factors are highly vulnerability to THZ1 treatment. We propose that downregulation of these transcription factors contributes, in part, to SCLC sensitivity to transcriptional inhibitors and that THZ1 represents a prototype drug for tailored SCLC therapy.

INTRODUCTION

Lung cancer accounts for nearly 30% of all cancer-related deaths. In 10–15% of lung cancer cases patients are diagnosed with small cell lung cancer (SCLC), the most malignant sub-type of lung cancer, characterized by aggressive growth, early onset of metastasis, and rapid development of chemo-refractory disease. The 5-year survival rate for SCLC patients is less than 5%—a poor prognosis that has not changed in four decades due to the lack of advancement in SCLC therapeutics (Sato et al., 2007; William and Glisson, 2011). In contrast to non-small cell lung cancer (NSCLC) where therapeutics designed to target known oncogenic drivers such as EGFR and ALK have been extremely effective; the poor understanding of SCLC disease etiology has precluded the identification of therapeutic targets and effective treatments (William and Glisson, 2011). Recent efforts to collect and sequence SCLC tissues have revealed that these tumors display a strikingly high rate of protein-changing mutations (Peifer et al., 2012; Rudin et al., 2012); however, paradoxically, no targetable mutations have been identified to guide therapeutic decisions for SCLC, and efficient treatment paradigms are urgently needed.

SCLC is defined by the near ubiquitous inactivation of both *P53* and *RB* (Peifer et al., 2012; Rudin et al., 2012; Sato et al., 2007); however, recent reports indicate that the cell of origin is equally important for the development of SCLC disease. Conditional inactivation of *P53* and *RB* in the adult mouse lung, using a genetically-engineered mouse (GEM) model, is sufficient to develop murine SCLC resembling human disease (Meuwissen et al., 2003). Importantly though, SCLC is only firmly established if P53 and RB is inactivated in the small population of pulmonary neuroendocrine cells (PNEC) (Sutherland et al., 2011). In contrast, P53 and RB loss confined to the abundant non-neuroendocrine cell population in the murine lungs cause low penetrance of SCLC and a significant increase in disease latency (Park et al., 2011; Sutherland et al., 2011). Thus, the PNEC is the major cell of origin of

SCLC, suggesting that neuroendocrine pathways collaborate with P53 and RB loss to initiate and drive SCLC tumorigenesis.

SCLC cells (as well as PNECs) exhibit high, sustained expression of many neuroendocrine genes, in particular transcription factors that regulate neuroendocrine development and differentiation in various tissues (Pedersen et al., 2003; Reynolds et al., 2000; Travis, 2009). Achaete-scute homolog 1 (ASCL1) which is a master regulator of neuroendocrine differentiation in lung development (Borges et al., 1997; Ito et al., 2000) and has been shown to regulate tumor-initiating capacity and survival pathways in SCLC (Jiang et al., 2009; Osada et al., 2005), hence underscoring the interplay between neuroendocrine signaling and SCLC pathogenesis. Furthermore, the lineage-specific transcription factor NEUROD1, has been reported to govern survival pathways in SCLC cells (Osborne et al., 2013). Further, SCLC cells exhibit various chromosomal and focal amplifications leading to increased target gene expression and possible gain-of-function. Fifty to eighty percent of SCLC tumors exhibit mutually exclusive amplification of the proto-oncogenes *MYC*, *MYCN*, or *MYCL* (Brennan et al., 1991; Huijbers et al., 2014; Johnson et al., 1987; Kim et al., 2006; Peifer et al., 2012; Rudin et al., 2012; Voortman et al., 2010). *MYC* is misregulated in the majority of human cancers leading to uncontrolled proliferation possible through augmentation of existing gene expression programs (Lin et al., 2012). In contrast to *MYC*, *MYCN* and *MYCL* misregulation occurs only in high-risk cancers of neuroendocrine origin such as SCLC (Huijbers et al., 2014; Johnson et al., 1987; McFadden et al., 2014), neuroblastoma (*MYCN*) (Huang and Weiss, 2013), and medulloblastoma (*MYCN*, *MYCL*) (Northcott et al., 2012). Moreover, many SCLC tumors have focal amplifications or increased expression of SOX-family genes (Voortman et al., 2010), including *SOX2*, which is critical for lung development and self-renewal. *SOX2* amplification and increased expression levels in tumors correlates with accelerated disease stage and silencing of SOX2 inhibits growth of SCLC cells (Rudin et al., 2012).

Thus, misregulated and amplified lineage-specific and proto-oncogenic transcription factors appear to govern SCLC initiation and disease evolution and downregulation of such factors could form the basis for SCLC targeted therapy.

Using an unbiased small molecule screen approach we indeed observed that SCLC is highly sensitive to transcription-targeting drugs and in particularly to a covalent inhibitor of cyclin-dependent kinase 7 (CDK7), THZ1, which can drastically reduce RNAPII-mediated gene transcription (Kwiatkowski et al., 2014). Here, we sought to investigate the therapeutic potential of THZ1 in SCLC pre-clinical models and further use THZ1 as a chemical tool to dissect the malignant transcriptional programs driving SCLC state.

RESULTS

High-throughput small-molecule drug screen identifies THZ1 as a highly potent inhibitor of SCLC viability

To identify small molecules that suppress SCLC cell growth we performed an unbiased high-throughput screen in SCLC cells lines using a library of greater than 1000 annotated small molecule inhibitors composed of both experimental compounds and early or advanced

clinical candidates. To minimize artefacts that may arise from long-term culture of SCLC cell lines we employed low-passage (passage 5–10), primary murine SCLC (mSCLC) cell lines, established from mSCLC tumors isolated from the GEM model of SCLC consisting of the $Rb^{L/L};p53^{L/L}$ (RP) allelic genotype (Meuwissen et al., 2003) (Figure 1A). To account for tumor heterogeneity, a total of 3 mSCLC cell lines (termed mSCLC1, 2, and 3), each from a different tumor-bearing RP mouse, were used to establish cell lines for the screen (Figure 1A). Importantly, all established mSCLC cell lines displayed morphology that is characteristic of SCLC by growing as suspension cells in floating aggregates and spheres (Figure 1A). Furthermore, the established mSCLC cells expressed classical SCLC-specific (neuroendocrine) markers (Figure S1A). Using a cell viability assay compounds were initially screened at a single dose on the mSCLC cells. Forty-five compounds elicited greater than 50% reduction in growth and were triaged for further inspection (Figure 1B). Fifteen compounds resulted in a mean anti-proliferation IC50 across 3 SCLC cell lines of less than 300 nM (Figure 1C). The top ranked inhibitors fell broadly into three major putative categories of inhibitors of 1) transcription (THZ1, Flavopiridol, CGP60474, JQ1, NVP-AUY922, 17-DMAG, BI2536), 2) cell cycle function (BI2536, CGP60474, AZD7762, ON-01910, PF477736, XMD16-144, THZ1), 3) mTOR-PI3K pathway (GSK2126458, PIK75, Torin 2) (Figure 1C–D).

SCLC cell lines demonstrate particular sensitivity to transcriptional inhibition with the top 3 scoring small molecule inhibitors from the screen (NVP-AUY922, BI2536, THZ1) targeting proteins involved in transcriptional regulation. NVP-AUY922 targets HSP90, which has recently been shown to be involved in regulating RNAPII pausing and transcriptional activation (Sawarkar et al., 2012). BI-2536, known as a polo-like 1 (PLK1) kinase inhibitor, has recently been shown to cross-react with bromodomain 4 (BRD4), a general co-activator of gene expression (Ember et al., 2014). The bromodomain (BRD) inhibitor JQ1 (Filippakopoulos et al., 2010) also ranked within the top-15 inhibitors (Figure 1C). Disappointingly however, despite displaying efficacy in tumor cell lines, clinical trials with both HSP90 inhibitors and PLK1 inhibitors have in general fared poorly. As a result, we focused much of our attention on THZ1, a recently identified covalent CDK7 inhibitor with additional cross reactivity against CDK12/13. THZ1 has recently been demonstrated to decrease T-cell acute lymphoblastic leukemia (T-ALL) viability, in part, through downregulation of key oncogenic transcription factors (Kwiatkowski et al., 2014). We speculated that the high ranking of THZ1 in the drug screen could indicate that SCLC exhibits similar dependencies for the expression of oncogenic transcription factors.

We compared the observed effects of THZ1 in murine SCLC cells with that of mutant *Kras*-driven murine NSCLC (mNSCLC) cell lines (Liu et al., 2013). THZ1 displayed an IC50 value of 75–100 nM against mSCLC cells, while mNSCLC cells were greater than 5-fold less sensitive to THZ1 treatment with IC50 around 1000 nM or greater (Figure 1E). These data suggest that lung cancer types addicted to mutated kinases are relatively less vulnerable to transcription-targeting drugs than SCLC. When testing several commercially available pan-CDK inhibitors targeting one or more of the higher-order transcriptional CDKs such as CDK7, 8, and 9, we found that apart from Flavopiridol and Dinaciclib, all compounds had an IC50 exceeding 500 or 1000 nM (Figure S1B–D). Dinaciclib and Flavopiridol showed

potency at a nanomolar scale similar to THZ1, but did not exhibit SCLC-specificity since *Kras*-driven NSCLC cell lines were equally sensitive to compounds (Figure S1B–C). As previously observed (Kwiatkowski et al., 2014), THZ1 facilitated irreversible (covalent) binding to CDK7 (Figure S1E) and a non-covalent version of THZ1 (THZ1-R) was significantly less potent (Figure S1F). Hence, THZ1 potently and selectively inhibits SCLC cell viability and its induced cellular effects results in part, in part, from its irreversible covalent inhibition of CDK7. Both Flavopiridol and THZ1 have been shown to cross react with CDK12/13 at higher concentrations (Bosken et al., 2014; Kwiatkowski et al., 2014), therefore this shared pharmacology may also impact the transcriptional and phenotypic response of SCLC to these inhibitors.

Mice with aggressive autochthonous SCLC disease show significant tumor response following THZ1 treatment

To establish the translational significance of the observed potency of THZ1 in SCLC cells, we tested THZ1 *in vivo* in the RP GEM model. This autochthonous mouse model offers a pre-clinical platform with remarkable resemblance to the human SCLC disease (Meuwissen et al., 2003). The concomitant loss of p53 and Rb function in the adult murine lung tissue allows for a stochastic and heterogeneous disease course with aggressively growing primary lung tumor and metastasis. Disease course in RP mice was followed by magnetic resonance imaging (MRI) of the thorax region, and upon detectable lung tumor burden, mice were started on treatment with either THZ1 or vehicle. We additionally treated a cohort of mice with Cisplatin and Etoposide (Cis-Eto) to allow for comparison to the standard-of-care chemotherapy regimen used in the clinic for SCLC patients. MRI was performed every two weeks after treatment start in the three different treatment cohorts (Figure 2A–F). All vehicle-treated mice showed progressive disease (PD – more than 20% increase in tumor volume compared to baseline) with up to more than doubling of tumor volume at the 2-week time point (Figure 2B, F). THZ1-treated mice had significant tumor response compared to control at the two-week time point (Figure 2B, C, F; Figure S2A). Three of nine THZ1-treated mice showed partial response (PR – more than 30% tumor volume reduction compared to baseline), and two of those had near-complete response with more than 90% reduction in tumor burden. Four THZ1-treated mice had stable disease (SD - neither reduction nor increase in tumor volume to classify as PR or PD), while two THZ1-treated mice had PD. Further, the majority of THZ1-treated mice with SD or PR at the two-week time point had similar disease responses at the four-week time point (Figure 2B–C, F, Figure S2A). In contrast, most vehicle-treated mice succumbed to their tumor burden before the four-week time point (4 out of 6 mice), emphasizing the aggressive disease course in the SCLC GEM model (Figure 2B, E). Overall, THZ1-treated mice had longer survival compared to control-treated mice ($p=0.0011$) (Figure 2E). Furthermore, we observed that response rates and survival obtained from single agent THZ1 treatment were comparable to tumor response rates upon standard-of-care chemotherapy (Figure 2B–F). However, THZ1 treatment did not result in treatment-related toxicity in RP mice in contrast to Cis-Eto treatment (Figure 2D). The lack of observed toxicity in THZ1-treated mice suggests that THZ1 treatment allows for a broader therapeutic window in cancer versus normal cells compared to chemotherapy.

To investigate whether single agent activity of THZ1 or Cis-Eto could be augmented by a combined treatment regimen, we treated an additional cohort of RP mice with THZ1 combined with Cis-Eto. Our results indicate that, THZ1-Cis-Eto treated mice do not experience superior tumor response at 4-week time point compared to mice receiving THZ1 or Cis-Eto alone (Figure S2B–E). Of note, we did not observe increased toxicity in THZ1-Cis-Eto treated mice compared to Cis-Eto treatment alone (Figure S2C).

THZ1 treatment resulted in decreased RNAPII CTD phosphorylation in SCLC tumor tissue as compared to vehicle-treated mice (Figure S2F) consistent with THZ1 binding and inhibition of CDK7 in tumor tissue. Tissue from both lung tumors (n=3) and liver metastases (n=1) isolated from THZ1-treated mice had significant more apoptotic cells than vehicle-treated tumor tissue as measured by TUNEL staining (Figure 2G, S2G). Additionally, mSCLC cells established from SCLC lung tumors and from liver metastases showed equal sensitivity to THZ1 indicating that both primary and metastatic SCLC lesions are responsive to THZ1 treatment (Figure 2H). Importantly, we found that mSCLC cells established from tumors from chemo-treated (resistant) SCLC RP mice had similar sensitivity to THZ1 when compared to mSCLC cell lines established from untreated (chemo-naïve) RP mice (Figure 2I). Thus, these data suggest that both chemo-naïve and –refractory SCLC disease is sensitive to THZ1 treatment.

Cellular and tumor models of human SCLC with distinct genotypes and phenotypes are highly sensitive to THZ1

To further confirm THZ1 as a drug candidate for patient disease we investigated THZ1 potency in a panel of genotypically-distinct human (hSCLC) cell lines. hSCLC cell lines are known to harbor a complex genome with high mutation rate, frequent copy number gains and losses, and translocations (Peifer et al., 2012; Pleasance et al., 2010; Rudin et al., 2012). The major identified alterations in the hSCLC cell lines, apart from the mutations in *P53* and *RB*, include amplification of *MYC*, *MYCL*, or *MYCN* (Johnson et al., 1987). We used a panel of hSCLC cell lines harboring amplifications in each of the *MYC* genes. Additionally, we investigated SCLC tumor cells from chemo-naïve and chemo-treated patients as well as those isolated from primary lung sites and from metastatic lesions (Figure 3A). All hSCLC cell lines exhibited high sensitivity to THZ1, with an IC50 in the range of 5–20 nM [Figure 3A (all), Figure 3B upper panel (representative)]. The NCI-H69, GLC16 and NCI-H82 cell lines established from chemo-treated patients were less sensitive to Cisplatin-Etoposide treatment than the chemo-naïve cell line NCI-H209 (Figure 3B lower panel). THZ1 treatment of tumor xenografts established from NCI-H69 and GLC16 cells resulted in significant tumor growth reduction compared to control-treated tumors, indicating that chemo-refractory disease is sensitive to THZ1 treatment (Figure 3C). As in GEM mice, no overt toxicity was observed from THZ1 treatment (Figure 3C, inserts). In contrast to hSCLC cells, immortalized tracheobronchial epithelial (hTBE) cells showed very little sensitivity to THZ1 but similar sensitivity to Cisplatin-Etoposide (Figure 3B), reinforcing previous observations that THZ1 treatment confers a superior therapeutic window between cancer and non-cancer cells compared to chemotherapy.

Significant induction of apoptosis was observed in hSCLC cells as early as 6 hours after exposure to THZ1 (Figure 3D) and significant inhibition of proliferation occurred at 24 and 48 hours after exposure (Figure 3E). The appearance of apoptotic markers appeared concomitant with decrease of RNAPII CTD phosphorylation (Figure 3D, F). In line with these results we observed that the classical sphere-forming morphology of SCLC cells was dramatically disrupted after only 12 hours exposure to THZ1 in 3D culture (Figure S3A). Similar differential sensitivity was observed between hSCLC and hNSCLC cells (Figure S3B–E), as previously noted in the murine cellular lung cancer models (Figure 1E). As observed in the mSCLC cell lines, most pan-CDK inhibitors tested showed either less potency in hSCLC cells or less SCLC-specificity (Figure S3C–E). Furthermore, we observed significantly lower potency of THZ1-R compared to THZ1, again confirming that the covalent mechanism of action of THZ1 is critical for drug potency (Figure S3F–G).

THZ1 confers preferential repression of transcription-regulating genes in SCLC cells

Intrigued by the significant therapeutic response in various preclinical models of SCLC disease, we aimed to understand the mechanisms governing SCLC sensitivity to THZ1. CDK7 is a component of the general transcription factor IIH (TFIIH), which activates RNAPII-mediated transcription. Consistent with this notion, high dose treatment with THZ1 in Jurkat cells was previously shown to cause pronounced global downregulation of gene expression; however, low dose THZ1 produced gene selective effects on the Jurkat interconnected transcriptional core regulatory circuitry (Kwiatkowski et al., 2014). To investigate THZ1-induced transcriptional effects in SCLC, we performed gene expression profiling in selected hSCLC cell lines; NCI-H69, GLC16 and NCI-H82; following treatment with 25 nM and 100 nM THZ1, which are concentrations at which limited and substantial inhibition of RNAPII phosphorylation are achieved, respectively (Figure 3F). Across SCLC cell lines, treatment with THZ1 led to a reduction in steady-state mRNA levels with 0.2–5% and 13–27% of mRNAs showing greater than 2-fold reduction at 25 and 100 nM, respectively (Figure 4A–B, Table S1, Table S2). Gene ontology (GO) analysis revealed a very significant enrichment of genes involved in transcription among the top-5% of downregulated genes after 100 nM THZ1 treatment (Figure 4C). In particular the major part of THZ1-sensitive transcripts is associated with DNA-dependent transcription indicating transcription factor function (Figure 4C). Moreover, gene set enrichment analysis of transcription factor binding sites showed that genes containing binding motifs for master regulatory transcription factors such as E2F, NRF1, and CREB were preferentially affected by THZ1 treatment (Figure S4A). In particular, we observed that short-lived transcripts of the E2F family were heavily downregulated and that E2F-regulated gene sets were significantly enriched in THZ1-downregulated transcripts (Figure S4B–C). Interestingly, E2F transcription factor binding sites are significantly enriched in the SCLC cells compared to the NSCLC (Figure S4D–E) suggesting that E2F transcription factors have a more prominent role in SCLC biology.

Proto-oncogenic and lineage-specific transcription factors are associated with super-enhancers in SCLC—Little is known about the transcription factors and co-factors that govern the pathogenesis of SCLC. Genes encoding important regulators of cell state, including key oncogenic transcription factors were recently shown to be preferentially

associated with unusually large transcriptional regulatory domains known as super-enhancers (Hnisz et al., 2013; Loven et al., 2013). Furthermore, previous work has demonstrated that expression of super-enhancer associated genes can be especially vulnerable to transcriptional inhibitors (Chapuy et al., 2013; Hnisz et al., 2013; Kwiatkowski et al., 2014; Loven et al., 2013; Whyte et al., 2013). Therefore the identification of super-enhancers in SCLC may enumerate candidate SCLC oncogenes and focus our search for THZ1-responsive transcripts whose downregulation lead to loss of SCLC cell state.

To identify super-enhancers in SCLC cells, we performed ChIP-seq against the lysine 27 acetylated form of histone H3 (H3K27Ac) in untreated hSCLC cells. H3K27Ac defines active enhancers and has been used previously to determine the position and size of super-enhancers (Hnisz et al., 2013). Using this approach, we identified 130 super-enhancer-associated genes in NCI-H69, 103 in GLC16, and 70 in NCI-H82 (Table S3, Figure 5A–D).

We found that many super-enhancer associated genes encode gene products involved in regulation of RNAPII-mediated transcription (Figure 5A, B). This indicates that many transcription factors are important to SCLC state and might represent candidate oncogenes. The super-enhancer landscape recapitulated the embryonic and neural signature common to SCLC cells. Many super-enhancers were found to be associated with genes encoding lineage-specific transcription factors that are central regulators of embryogenesis and neural development (Figure 5A–B). Consistent with previous investigations observing differential gene expression profiles between the so-called ‘classical’ and ‘variant’ SCLC cell lines (Johnson et al., 1987; Pedersen et al., 2003) we found that the ‘classical’ GLC16 and NCI-H69 cell lines had significant overlap in identified super-enhancer genes while the ‘variant’ NCI-H82 cell line had a distinct super-enhancer profile from the classical cell lines (Figure 5B–C).

In both NCI-H69 and GLC16 cell lines, we identified super-enhancers associated with *SOX2* and *NFIB* (Figure 5A, D) consistent with their proposed role as proto-oncogenic transcription factors in SCLC (Dooley et al., 2011; Rudin et al., 2012). Similarly, the neuroendocrine master transcription factor gene *ASCL1* (Borges et al., 1997; Ito et al., 2000) was associated with one of the largest typical enhancers (Figure 5A, D, Table S2). Moreover, we identified many super-enhancer associated transcription factor genes in GLC16 and NCI-H69 whose functions were not previously described in the context of SCLC biology. Among them was *Insulinoma-associated 1* (*INSM1*) (Figure 5A, D, Table S3), which represent a highly predictive marker of SCLC disease (Figure S5) (Christensen et al., 2010; Lan and Breslin, 2009; Pedersen et al., 2003). In the NCI-H82 cell line, we identified a super-enhancer at the *OTX2* gene, which encodes a transcription factor involved in neural differentiation and development. Similar to *INSM1*, the functional role of *OTX2* in SCLC biology is unknown. Moreover, we identified large typical enhancers associated with the proto-oncogenic neuroendocrine transcription factor genes *NEUROD1* (Figure 5A, D, S5, Table S3) (Osborne et al., 2013).

Super-enhancers were found to be associated with genes that had focal amplification. The *C-MYC* amplified cell lines GLC16 and NCI-H82 and the *MYCN* amplified cell line NCI-H69 (Figure 3A) had super-enhancers associated with *C-MYC* and *MYCN* gene loci respectively

(Figure 5A, 5D). In the NCI-H69 cell lines the *MYCN* super-enhancer ranked second largest and in NCI-H82 the two largest super-enhancers were both found in the C-MYC gene loci (Table S3). Interestingly, we in addition found evidence for focal amplification of *OTX2* in the NCI-H82 cell line (Figure 5D).

Super-enhancer associated genes are disproportionally vulnerable to THZ1 treatment

Next we aimed to investigate whether THZ1 conferred preferential repression of super-enhancer associated genes in SCLC (Figure 6A–C). Enrichment analysis of THZ1-sensitive transcripts (Figure 4, Table S2) and super-enhancer associated genes (Table S3) showed that THZ1-targeted transcripts are enriched in the gene sets with associated super-enhancers (FDR<0.05) (Figure 6A, Table S4). Moreover, mean transcript abundance associated with super-enhancers (SEs) was disproportionately reduced upon THZ1 exposure compared to that of typical enhancers (TEs) (Figure 6B). This disproportionate reduction was observed even at the low dose (25 nM) of THZ1, which produces limited repression of RNAPII-mediated transcription (Figure 3F). In addition genes associated with the top ranked (largest) TE (TOPTE) were more sensitive to THZ1 treatment than genes associated with a general TE (Figure 6B) emphasizing that enhancer size is positively correlated with THZ1 vulnerability.

In order to focus our search for SCLC oncogenic transcription factors we identified a leading-edge gene set consisting of super-enhancer associated transcripts that were significantly downregulated by THZ1 (Figure 6C). As oncogenic transcription factors are often highly expressed we further filtered our leading-edge gene set (Figure 6C) to contain the top 5 % actively expressed genes (Figure 6D). Confirmative of this scheme, *MYC*-family of proto-oncogenes placed among the leading-edge gene set and was among the top 5 % most actively expressed genes in the analyzed hSCLC cells (Figure 6D). Using this approach we further identified *SOX2*, *SOX4*, *NFIB*, *INSM1* (NCI-H69, GLC16) and *OTX2* (NCI-H82). *ASCL1* (NCI-H69, GLC16) and *NEUROD1* (NCI-H82) both associated with a TOPTE, but were both highly reduced in THZ1-treated cells and ranked among the top 5 % actively expressed genes (Figure 6C–D). The downregulation of the transcription factor genes were confirmed on RNA level by quantitative PCR (Figure 6E) and selected transcripts further confirmed on protein level (Figure 6F). The reduced transcript level of SCLC-specific transcription factors observed *in vitro* was furthermore confirmed *in vivo* in THZ1-treated RP mice (Figure S6).

DISCUSSION

Here, we addressed a high therapeutic need by identifying THZ1 (Kwiatkowski et al., 2014), as a promising drug candidate for the treatment of SCLC. While recent sequencing efforts revealed that SCLC tumors contain a high rate of protein-altering mutations, the mapping of the mutational landscape did not guide in therapeutic decisions for this fatal disease (Peifer et al., 2012; Rudin et al., 2012). Using an unbiased small molecule screen approach we observed that SCLC cells were highly vulnerable to perturbation of the transcriptional state since several transcriptional inhibitors were potent inhibitors of SCLC cell viability. The high potency of THZ1 in SCLC cells was further confirmed *in vivo* in the RP GEM mice

model, which represents a highly translational preclinical platform for the investigation of SCLC therapeutics (Meuwissen et al., 2003). The RP GEM model mimics the stochastic and heterogeneous pathogenesis in human disease and mSCLC tumors have been shown to accumulate additional alterations as observed in human disease, such as amplification of *MYCL* (McFadden et al., 2014; Peifer et al., 2012). We observed significant tumor responses in SCLC GEM mice treated with THZ1 compared to control-treated mice and further noted that standard-of-care chemotherapy caused similar response rates in SCLC GEM mice. However, while chemotherapy was associated with toxicity, THZ1 treatment did not cause any overt toxicity in treated mice. Furthermore our treatment data in both murine and human pre-clinical models of SCLC indicate that both metastatic and chemo-refractory SCLC disease is sensitive to THZ1 treatment.

The encouraging preclinical results led us to investigate the transcriptional addictions of SCLC. Due to the preponderance of misregulated transcription factors in SCLC (Dooley et al., 2011; Jiang et al., 2009; Johnson et al., 1987; Osborne et al., 2013; Pedersen et al., 2003; Rudin et al., 2012; Voortman et al., 2010), we aimed to identify a candidate list of transcription factor genes associated with super-enhancers (Chapuy et al., 2013; Hnisz et al., 2013; Kwiatkowski et al., 2014; Loven et al., 2013; Whyte et al., 2013) and whose high-level expression were particular vulnerable to THZ1 treatment. We hypothesized that such a list would represent candidate oncogenic transcription factors in SCLC disease.

Affirmative of this scheme, we identified that the focally amplified *C-MYC* (in GLC16 and NCI-H82 cells) and *MYCN* (in NCI-H69 cells) proto-oncogenes (Brennan et al., 1991; Voortman et al., 2010)were associated with large super-enhancers and were highly vulnerable to THZ1. We did not observe differential sensitivity to THZ1 between SCLC cells with genomic amplification of either *MYCN*, *C-MYC*, or *MYCL* and cell lines without amplification, therefore suggesting that *MYC* amplification is not a biomarker *per se* for THZ1-sensitive SCLC. Since focal amplification of *MYC* gene members is associated with later-stage disease and, possibly, chemo-resistant disease (Brennan et al., 1991; Johnson et al., 1987), these data further support that THZ1 treatment will be effective in progressive aggressive SCLC disease stages.

In contrast to *MYC* amplifications, the transcriptional-amplified neuroendocrine gene program is an early and possible contributing event of SCLC disease, in which PNECs are believed to be the cell of origin (Park et al., 2011; Sutherland et al., 2011). The PNECs are abundant in the developing lung, where they play a role in lung branching morphogenesis and oxygen sensing. The purpose and function of the small population (<0.5 %) of PNECs maintained in the adult lung epithelium is not known (Reynolds et al., 2000; Travis, 2009). While the neuroendocrine signature of SCLC has been a central diagnostic tool only few functional studies have been performed to explore if and how the malignant neuroendocrine factors contribute to SCLC disease (Ball, 2004; Lan and Breslin, 2009). We identified a top-ranked (large) typical enhancer (TOPTE) associated with *ASCL1*, in support of its established role as a master transcription factor in lung neuroendocrine differentiation (Borges et al., 1997) and as a proposed candidate oncogene in SCLC (Jiang et al., 2009). Our results greatly corroborate these findings as we observe that *ASCL1* is among the top-2% most downregulated genes in THZ1-treated cells. We further identified several

candidate oncogenic transcription factors in SCLC. One example is the neuroendocrine transcription factor INSM1, which is represent a highly lineage-defining trait of SCLC. INSM1 phenocopies ASCL1 function in murine neural development but it is not known whether same functional link exist in SCLC biology (Ball, 2004; Lan and Breslin, 2009). Future work should investigate the role of INSM1 and other transcription factors in the malignant transcriptional gene programs that drive and maintain SCLC disease.

Our chemical screen revealed that 7 out of 15 compounds identified as potent inhibitors of SCLC cell viability are transcriptional inhibitors. Hence, further pharmacological studies of small molecules targeting the general transcription apparatus, should be performed to advance the field of SCLC-tailored therapeutics and to uncover the transcriptional addictions of SCLC.

EXPERIMENTAL PROCEDURES

Generation of genetically engineered mouse (GEM) model of SCLC and murine SCLC cell lines

Mice were bred to contain conditional *p53* floxed (L) allele (Jonkers et al., 2001) and *Rb* floxed (L) allele (Meuwissen et al., 2003) to a final genotype of $Rb^{L/L}$;$p53^{L/L}$ (RP). All experimental mice were maintained on a mixed genetic background (C57Bl/6, Balb-c, and S129). From 6 weeks of age mice were induced with Adenovirus-Cre recombinase (Ad-Cre) by intratracheal intubation (DuPage et al., 2009) to allow for cre-lox mediated recombination of floxed *p53* and *Rb* alleles. Mice were aged 8–12 months to allow for SCLC disease development. The Animal Care and Use Committee of the Dana-Farber Cancer Institute approved all *in vivo* experiments performed in this study. Murine SCLC cell lines (mSCLC) were established from RP tumors upon mechanical dissection of tissue. Cells were established and maintained in HITES medium (Carney et al., 1981) with 10 % FBS and cultured at 37°C in a humidified chamber with 5 % CO_2. Extracted DNA from cell lines were evaluated for *p53* and *Rb* recombination as previously described (Jonkers et al., 2001; Meuwissen et al., 2003). Cell stocks were frozen at very low passage (p=5) for use in screen experiments.

High-throughput small molecule screen

Using a semi-automated platform we tested >1000 small molecule annotated library. in 3 mSCLC cell lines (termed mSCLC1, 2, and 3). Cells were seeded in a 384-well format and treated with a concentration of 600 nM of individual compounds before evaluating cell viability after 120 hours (2 doubling times) using CellTiter-Glo Lumeniscent assay (Promega). Further evaluation of compounds which allowed for more than 50% inhibition of cell viability was performed in a 5-point 2-fold dilution series of each compound before evaluating cell viability after 120 hours using CellTiter-Glo (experimental repeat 1) or MTS-based CKK-8 assay (Dojindo) (experimental repeat 2).

See Supplemental Experimental Procedures.

Genetically engineered mice (GEM) dosing studies and Magnetic Resonance Imaging—Mice were imaged on a 7 Tesla BioSpec; Bruker BioSpin) with MRI protocols

optimized for image requisition of pulmonary parenchyma and vessels in healthy mice. Upon determination of tumor growth mice were randomized into treatment groups receiving either THZ (Kwiatkowski et al., 2014), Cisplatin-Etoposide or vehicle.

See Supplemental Experimental Procedures.

RNA extraction and Synthetic RNA Spike-In

In short, total RNA from human SCLC cells was prepared using ERCC RNA Spike-In Mix (Ambion) as previously described (Loven et al., 2012).

See supplemental Experimental Procedures

Microarray Sample Preparation and Analysis

Gene expression analysis on spiked-in RNA samples was performed using Human PrimeView array (Affymetrix) as previously described (Kwiatkowski et al., 2014).

See supplemental Experimental Procedures

Chromatin Immunoprecipitation, sequencing and analysis

Human SCLC cells were cross-linked and incubated with magnetic bead bound-antibody for H3K27Ac (Abcam) before sonication to achieve DNA fragment of 200–250 basepair. Crosslinks of precipitated protein-DNA complexes were hereafter reversed and sequencing was performed using Illumina HiSeq 2000.

See Supplemental Experimental Procedures.

Supplementary Material

Refer to Web version on PubMed Central for supplementary material.

Acknowledgments

This work was supported by a Post-Doctoral Fellowship - R56-A3106-12-S2 - from the Danish Cancer Society (C.L.C); Deutsche Forschungsgemeinschaft - HE6897/1-1 (G.H.S.), the NIH grants CA122794, CA140594, CA163896, CA166480, CA154303, and CA120964 (K.K.W.), the R01 CA179483-01A1 (N.S.G.), the Thoracic Foundation (K.K.W), the Susan Spooner Foundation (K.K.W.) and the MIT-DFCI Bridge grant (K.K.W, N.S.G, R.A.Y).

References

Ball DW. Achaete-scute homolog-1 and Notch in lung neuroendocrine development and cancer. Cancer letters. 2004; 204:159–169. [PubMed: 15013215]

Borges M, Linnoila RI, van de Velde HJ, Chen H, Nelkin BD, Mabry M, Baylin SB, Ball DW. An achaete-scute homologue essential for neuroendocrine differentiation in the lung. Nature. 1997; 386:852–855. [PubMed: 9126746]

Bosken CA, Farnung L, Hintermair C, Merzel Schachter M, Vogel-Bachmayr K, Blazek D, Anand K, Fisher RP, Eick D, Geyer M. The structure and substrate specificity of human Cdk12/Cyclin K. Nature communications. 2014; 5:3505.

Brennan J, O'Connor T, Makuch RW, Simmons AM, Russell E, Linnoila RI, Phelps RM, Gazdar AF, Ihde DC, Johnson BE. myc family DNA amplification in 107 tumors and tumor cell lines from

patients with small cell lung cancer treated with different combination chemotherapy regimens. Cancer research. 1991; 51:1708–1712. [PubMed: 1847842]

Carney DN, Bunn PA Jr, Gazdar AF, Pagan JA, Minna JD. Selective growth in serum-free hormone-supplemented medium of tumor cells obtained by biopsy from patients with small cell carcinoma of the lung. Proceedings of the National Academy of Sciences of the United States of America. 1981; 78:3185–3189. [PubMed: 6265940]

Chapuy B, McKeown MR, Lin CY, Monti S, Roemer MG, Qi J, Rahl PB, Sun HH, Yeda KT, Doench JG, et al. Discovery and characterization of super-enhancer-associated dependencies in diffuse large B cell lymphoma. Cancer cell. 2013; 24:777–790. [PubMed: 24332044]

Christensen CL, Gjetting T, Poulsen TT, Cramer F, Roth JA, Poulsen HS. Targeted cytosine deaminase-uracil phosphoribosyl transferase suicide gene therapy induces small cell lung cancer-specific cytotoxicity and tumor growth delay. Clinical cancer research : an official journal of the American Association for Cancer Research. 2010; 16:2308–2319. [PubMed: 20371678]

Dooley AL, Winslow MM, Chiang DY, Banerji S, Stransky N, Dayton TL, Snyder EL, Senna S, Whittaker CA, Bronson RT, et al. Nuclear factor I/B is an oncogene in small cell lung cancer. Genes & development. 2011; 25:1470–1475. [PubMed: 21764851]

DuPage M, Dooley AL, Jacks T. Conditional mouse lung cancer models using adenoviral or lentiviral delivery of Cre recombinase. Nature protocols. 2009; 4:1064–1072.

Ember SW, Zhu JY, Olesen SH, Martin MP, Becker A, Berndt N, Georg GI, Schonbrunn E. Acetyl-lysine Binding Site of Bromodomain-Containing Protein 4 (BRD4) Interacts with Diverse Kinase Inhibitors. ACS chemical biology. 2014

Filippakopoulos P, Qi J, Picaud S, Shen Y, Smith WB, Fedorov O, Morse EM, Keates T, Hickman TT, Felletar I, et al. Selective inhibition of BET bromodomains. Nature. 2010; 468:1067–1073. [PubMed: 20871596]

Hnisz D, Abraham BJ, Lee TI, Lau A, Saint-Andre V, Sigova AA, Hoke HA, Young RA. Super-enhancers in the control of cell identity and disease. Cell. 2013; 155:934–947. [PubMed: 24119843]

Huang M, Weiss WA. Neuroblastoma and MYCN. Cold Spring Harbor perspectives in medicine. 2013; 3:a014415. [PubMed: 24086065]

Huijbers IJ, Bin Ali R, Pritchard C, Cozijnsen M, Kwon MC, Proost N, Song JY, de Vries H, Badhai J, Sutherland K, et al. Rapid target gene validation in complex cancer mouse models using re-derived embryonic stem cells. EMBO molecular medicine. 2014; 6:212–225. [PubMed: 24401838]

Ito T, Udaka N, Yazawa T, Okudela K, Hayashi H, Sudo T, Guillemot F, Kageyama R, Kitamura H. Basic helix-loop-helix transcription factors regulate the neuroendocrine differentiation of fetal mouse pulmonary epithelium. Development. 2000; 127:3913–3921. [PubMed: 10952889]

Jiang T, Collins BJ, Jin N, Watkins DN, Brock MV, Matsui W, Nelkin BD, Ball DW. Achaete-scute complex homologue 1 regulates tumor-initiating capacity in human small cell lung cancer. Cancer research. 2009; 69:845–854. [PubMed: 19176379]

Johnson BE, Ihde DC, Makuch RW, Gazdar AF, Carney DN, Oie H, Russell E, Nau MM, Minna JD. myc family oncogene amplification in tumor cell lines established from small cell lung cancer patients and its relationship to clinical status and course. The Journal of clinical investigation. 1987; 79:1629–1634. [PubMed: 3034978]

Jonkers J, Meuwissen R, van der Gulden H, Peterse H, van der Valk M, Berns A. Synergistic tumor suppressor activity of BRCA2 and p53 in a conditional mouse model for breast cancer. Nature genetics. 2001; 29:418–425. [PubMed: 11694875]

Kim YH, Girard L, Giacomini CP, Wang P, Hernandez-Boussard T, Tibshirani R, Minna JD, Pollack JR. Combined microarray analysis of small cell lung cancer reveals altered apoptotic balance and distinct expression signatures of MYC family gene amplification. Oncogene. 2006; 25:130–138. [PubMed: 16116477]

Kwiatkowski N, Zhang T, Rahl PB, Abraham BJ, Reddy J, Ficarro SB, Dastur A, Amzallag A, Ramaswamy S, Tesar B, et al. Targeting transcription regulation in cancer with a covalent CDK7 inhibitor. Nature. 2014; 511:616–620. [PubMed: 25043025]

Lan MS, Breslin MB. Structure, expression, and biological function of INSM1 transcription factor in neuroendocrine differentiation. FASEB journal : official publication of the Federation of American Societies for Experimental Biology. 2009; 23:2024–2033. [PubMed: 19246490]

Lin CY, Loven J, Rahl PB, Paranal RM, Burge CB, Bradner JE, Lee TI, Young RA. Transcriptional amplification in tumor cells with elevated c-Myc. Cell. 2012; 151:56–67. [PubMed: 23021215]

Liu Y, Marks K, Cowley GS, Carretero J, Liu Q, Nieland TJ, Xu C, Cohoon TJ, Gao P, Zhang Y, et al. Metabolic and functional genomic studies identify deoxythymidylate kinase as a target in LKB1-mutant lung cancer. Cancer discovery. 2013; 3:870–879. [PubMed: 23715154]

Loven J, Hoke HA, Lin CY, Lau A, Orlando DA, Vakoc CR, Bradner JE, Lee TI, Young RA. Selective inhibition of tumor oncogenes by disruption of super-enhancers. Cell. 2013; 153:320–334. [PubMed: 23582323]

Loven J, Orlando DA, Sigova AA, Lin CY, Rahl PB, Burge CB, Levens DL, Lee TI, Young RA. Revisiting global gene expression analysis. Cell. 2012; 151:476–482. [PubMed: 23101621]

McFadden DG, Papagiannakopoulos T, Taylor-Weiner A, Stewart C, Carter SL, Cibulskis K, Bhutkar A, McKenna A, Dooley A, Vernon A, et al. Genetic and clonal dissection of murine small cell lung carcinoma progression by genome sequencing. Cell. 2014; 156:1298–1311. [PubMed: 24630729]

Meuwissen R, Linn SC, Linnoila RI, Zevenhoven J, Mooi WJ, Berns A. Induction of small cell lung cancer by somatic inactivation of both Trp53 and Rb1 in a conditional mouse model. Cancer cell. 2003; 4:181–189. [PubMed: 14522252]

Northcott PA, Shih DJ, Peacock J, Garzia L, Morrissy AS, Zichner T, Stutz AM, Korshunov A, Reimand J, Schumacher SE, et al. Subgroup-specific structural variation across 1,000 medulloblastoma genomes. Nature. 2012; 488:49–56. [PubMed: 22832581]

Osada H, Tatematsu Y, Yatabe Y, Horio Y, Takahashi T. ASH1 gene is a specific therapeutic target for lung cancers with neuroendocrine features. Cancer research. 2005; 65:10680–10685. [PubMed: 16322211]

Osborne JK, Larsen JE, Shields MD, Gonzales JX, Shames DS, Sato M, Kulkarni A, Wistuba II, Girard L, Minna JD, Cobb MH. NeuroD1 regulates survival and migration of neuroendocrine lung carcinomas via signaling molecules TrkB and NCAM. Proceedings of the National Academy of Sciences of the United States of America. 2013; 110:6524–6529. [PubMed: 23553831]

Park KS, Liang MC, Raiser DM, Zamponi R, Roach RR, Curtis SJ, Walton Z, Schaffer BE, Roake CM, Zmoos AF, et al. Characterization of the cell of origin for small cell lung cancer. Cell cycle. 2011; 10:2806–2815. [PubMed: 21822053]

Pedersen N, Mortensen S, Sorensen SB, Pedersen MW, Rieneck K, Bovin LF, Poulsen HS. Transcriptional gene expression profiling of small cell lung cancer cells. Cancer research. 2003; 63:1943–1953. [PubMed: 12702587]

Peifer M, Fernandez-Cuesta L, Sos ML, George J, Seidel D, Kasper LH, Plenker D, Leenders F, Sun R, Zander T, et al. Integrative genome analyses identify key somatic driver mutations of small-cell lung cancer. Nature genetics. 2012; 44:1104–1110. [PubMed: 22941188]

Pleasance ED, Stephens PJ, O'Meara S, McBride DJ, Meynert A, Jones D, Lin ML, Beare D, Lau KW, Greenman C, et al. A small-cell lung cancer genome with complex signatures of tobacco exposure. Nature. 2010; 463:184–190. [PubMed: 20016488]

Reynolds SD, Giangreco A, Power JH, Stripp BR. Neuroepithelial bodies of pulmonary airways serve as a reservoir of progenitor cells capable of epithelial regeneration. The American journal of pathology. 2000; 156:269–278. [PubMed: 10623675]

Rudin CM, Durinck S, Stawiski EW, Poirier JT, Modrusan Z, Shames DS, Bergbower EA, Guan Y, Shin J, Guillory J, et al. Comprehensive genomic analysis identifies SOX2 as a frequently amplified gene in small-cell lung cancer. Nature genetics. 2012; 44:1111–1116. [PubMed: 22941189]

Sato M, Shames DS, Gazdar AF, Minna JD. A translational view of the molecular pathogenesis of lung cancer. Journal of thoracic oncology : official publication of the International Association for the Study of Lung Cancer. 2007; 2:327–343.

Sawarkar R, Sievers C, Paro R. Hsp90 globally targets paused RNA polymerase to regulate gene expression in response to environmental stimuli. Cell. 2012; 149:807–818. [PubMed: 22579285]

Sutherland KD, Proost N, Brouns I, Adriaensen D, Song JY, Berns A. Cell of origin of small cell lung cancer: inactivation of Trp53 and Rb1 in distinct cell types of adult mouse lung. Cancer cell. 2011; 19:754–764. [PubMed: 21665149]

Travis WD. Lung tumours with neuroendocrine differentiation. European journal of cancer. 2009; 45(Suppl 1):251–266. [PubMed: 19775623]

Voortman J, Lee JH, Killian JK, Suuriniemi M, Wang Y, Lucchi M, Smith WI Jr, Meltzer P, Wang Y, Giaccone G. Array comparative genomic hybridization-based characterization of genetic alterations in pulmonary neuroendocrine tumors. Proceedings of the National Academy of Sciences of the United States of America. 2010; 107:13040–13045. [PubMed: 20615970]

Whyte WA, Orlando DA, Hnisz D, Abraham BJ, Lin CY, Kagey MH, Rahl PB, Lee TI, Young RA. Master transcription factors and mediator establish super-enhancers at key cell identity genes. Cell. 2013; 153:307–319. [PubMed: 23582322]

William WN Jr, Glisson BS. Novel strategies for the treatment of small-cell lung carcinoma. Nature reviews Clinical oncology. 2011; 8:611–619.

SIGNIFICANCE

In contrast to other lung carcinomas, there has been no significant progress in the development of SCLC therapies since the introduction of chemotherapy in the 1970s. Although SCLC tumors exhibit a complex genome with a high mutation rate, genomic characterization of SCLC has thus far not revealed druggable oncogenes. Here we find that inhibitors of the general transcription apparatus, including a covalent inhibitor of CDK7 (THZ1), potently suppress SCLC growth. We identify a number of THZ1-responsive transcripts, including super-enhancer-associated proto-oncogenic and lineage-specific transcription factors, whose vulnerability to THZ1 contributes to SCLC sensitivity. Our data suggests that THZ1 can effectively target these candidate SCLC proto-oncogenes leading to a viable therapeutic window for effective SCLC therapy.

HIGHLIGHTS

- SCLC is vulnerable to inhibition of RNAPII-mediated transcription by THZ1
- SCLC super-enhancers associate with proto-oncogenes and key SCLC identity genes
- THZ1 preferentially targets super-enhancer-driven transcription factor genes
- THZ1 represents a promising experimental agent for the treatment of SCLC

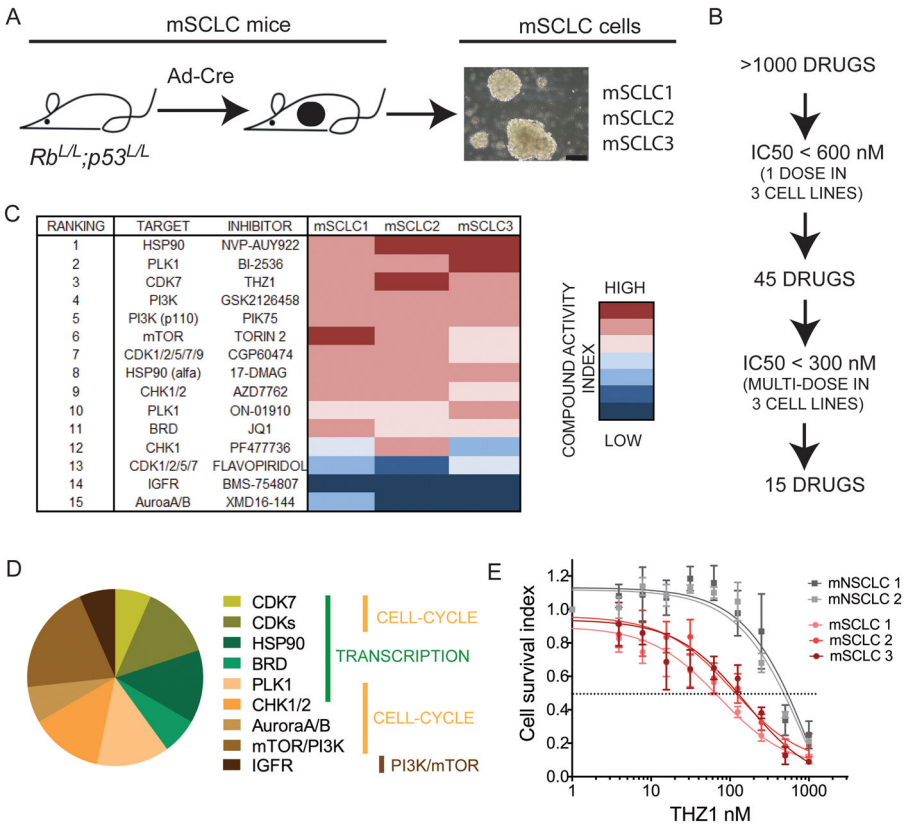

Figure 1. High-throughput drug screen in primary murine SCLC cell lines identifies THZ1 as a highly potent inhibitor of SCLC cell viability

A) Murine SCLC cell lines (mSCLC1, mSCLC2, mSCLC3) were established from 3 different adenovirus-Cre recombinase (Ad-Cre)-induced $Rb^{L/L};p53^{L/L}$ (RP) mice aged 8–10 months. Representative morphology of established primary mSCLC cells is shown to the right in the panel. Black scale bar shown in micrographs represent 50μm.

B) >1000 small-molecule inhibitors were included in a high-throughput screen using mSCLC1, mSCLC2 and mSCLC3 cell lines at passage 5–10. All drugs were added to each cell line (day 0) at a concentration of 600 nM, and cell viability was measured at day 5, allowing for 2 doubling cycles of (control) cells. The inhibitors, which reduced cell viability by 50 % (compared to no drug control), were further ranked following dose escalation treatment to determine IC50 of cell viability. Fifteen compounds had an IC50 below 300 nM according to both cell viability assays.

C) Summary of top-15 ranked small molecules and corresponding targets as represented in an ‘IC50 heatmap’ format.

D) Distribution of putative targets of top-15 ranked small molecules with targets categorized as regulating 1) transcription (indicated with green bar), 2) cell cycle (yellow bar) or 3) PI3K-mTOR pathway (brown bar).

E) mSCLC and mNSCLC cell lines (mNSCLC1: $Kras^{+/LSL\text{-}G12D};p53^{L/L}$, mNSCLC2: $Kras^{+/LSL\text{-}G12;};p53^{L/L};Lkb1^{L/L}$) were incubated with increasing doses of THZ1 and IC50 were measured by cell viability assay. Data are presented as mean +/− SEM.

See also Figure S1.

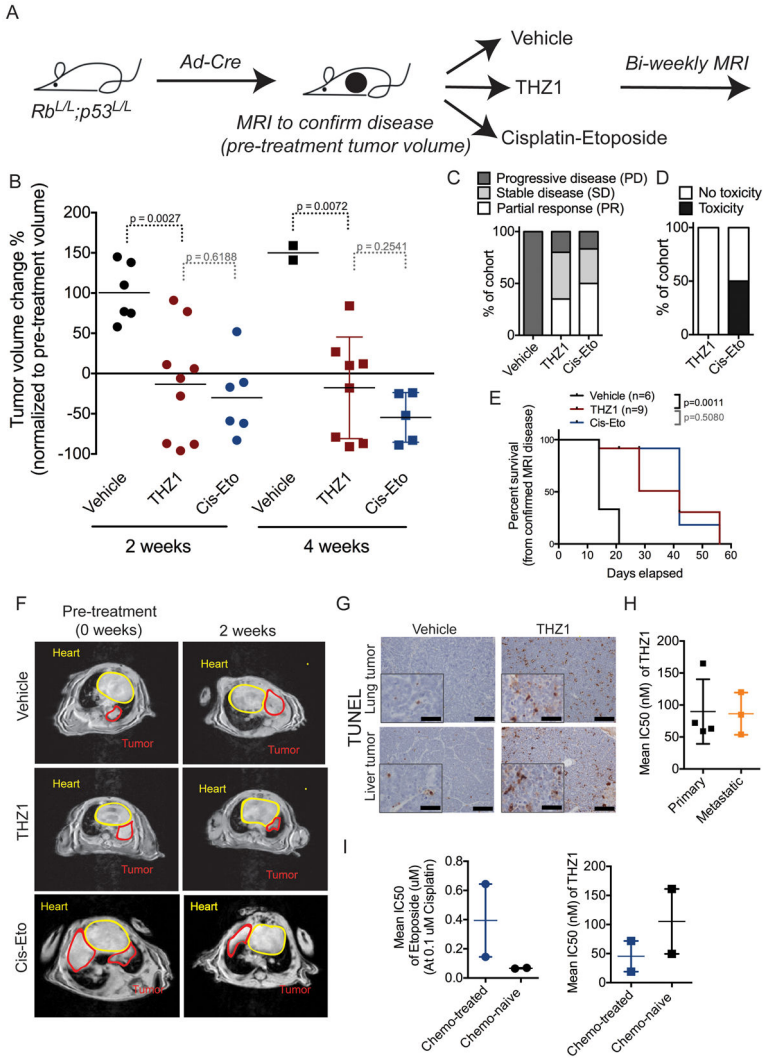

Figure 2. THZ1 treatment of RP mice causes significant tumor response and increased survival

A) Schematic overview of treatment trial with vehicle (control), THZ1 or Cisplatin-Etoposide compared to vehicle (control) in RP mice with confirmed (by MRI) SCLC disease. THZ1 is dosed at 10 mg/kg BID, Cisplatin-Etoposide (Cis-Eto) is dosed as follow: Cisplatin 5 mg/kg 1x per week, Etoposide 10 mg/kg 3x per week. Cis-Eto is given 1–2 weeks *on* (pending weight/toxicity) hereafter 2–3 weeks *off* followed by 1–2 weeks re-treatment (pending weight/toxicity and tumor burden according to MRI). After treatment start MRI was performed biweekly in all treatment cohorts.

B) Tumor volume changes (%) according to MRI quantification in vehicle-treated (control), THZ1-treated and Cisplatin-Etoposide-treated mice at 2 and 4 weeks as normalized to pre-treatment (week 0) tumor volume. p-values between different treatment cohorts were calculated using Students t-test. Data are shown as individual values for tumor volume change (dots or squares) with horizontal line representing mean.

C) Treatment response as divided into PD (progressive disease), SD (stable disease), and PR (partial response) groups in mice treated with vehicle (control), THZ1 or Cis-Eto. Data is shown as percent of total mice in respective treatment cohort.

D) Toxicity events observed in mice treated with THZ1 or Cis-Eto as measured by weight loss in mice. If an animal's weight decreased to 15 % or below (compared to pre-treatment weight) during the treatment study, animal was recorded to have treatment-induced toxicity. Data is shown as percent (%) of total mice in treatment cohort.

E) Survival of control, THZ1-treated and Cis-Eto-treated mice. p-value was established using log-rank test (Mantel-Cox test).

F) Representative MRIs of thorax region of mice treated with vehicle (control), THZ1 or Cis-Eto at 2 and 4 weeks.

G) Representative 20x field micrographs (inserts 40x field) of Terminal deoxynucleotidyl transferase dUTP nick end-labeling (TUNEL) staining of lung tumor and liver metastases 72 hours after treatment with THZ1 or vehicle. Black scale bar in micrographs (20x) represent 50μm. Black scale bar in insert (40x) represent 25μm.

H) Primary (lung) and metastatic (liver) SCLC lesions were isolated from Ad-Cre induced RP mice for cell line establishment. Cells established from lung tumor (primary) and metastatic (liver tumor) origin were incubated with increasing doses of THZ1, and the IC50s were determined by cell viability assay. IC50 from several different cell lines of either group are plotted to give a total calculated mean IC50 (horizontal line) with error bars representing SEM.

I) SCLC tumor lesions from the lung were isolated from untreated RP mice (n=2) and chemo-treated mice (n=2) for establishment of primary cell lines. Primary cells (at passage 5) were incubated with increasing doses of Cis-Eto (right) or THZ1 (left) and the IC50s were determined by cell viability assay. IC50 from several different cell lines of either group are plotted (squares or dots) to give a total calculated mean IC50 (horizontal line) with error bars representing SEM.

See also Figure S2.

A

Cell line	Phenotype profile: Origin	Phenotype profile: Chemotherapy	Genetic profile: *P53* mut	Genetic profile: *RB* mut	Genetic profile: *MYC* amp	IC50 [CI] nM
NCI-H69	Pleural effusion	yes	mut	mut	*MYCN*	7 [4;10]
GLC16	Lung biopsy	yes	mut	mut	*C-MYC*	8 [6;12]
GLC19	Lung biopsy	yes	mut	mut	*C-MYC*	9 [5;14]
NCI-H2171	Lung biopsy	yes	mut	mut	*C-MYC*	7 [4;18]
GLC26	Lung biopsy	yes	mut	mut	*MYCL*	8 [6;14]
DMS153	Liver	yes	mut	mut	*MYCL*	13 [9;18]
DMS79	Lung	yes	mut	mut	none	5 [3;8]
DMS92	Bone marrow	no	mut	mut	none	18 [15;27]
NCI-H209	Bone marrow	no	mut	mut	none	5 [3;11]
NCI-H82*	Pleural effusion	yes	mut	mut	*C-MYC*	10 [4;27]
GLC2*	Pleural effusion	no	mut	mut	*C-MYC*	20 [10;32]
GLC3*	Pleural effusion	no	mut	mut	*C-MYC*	11 [8;19]

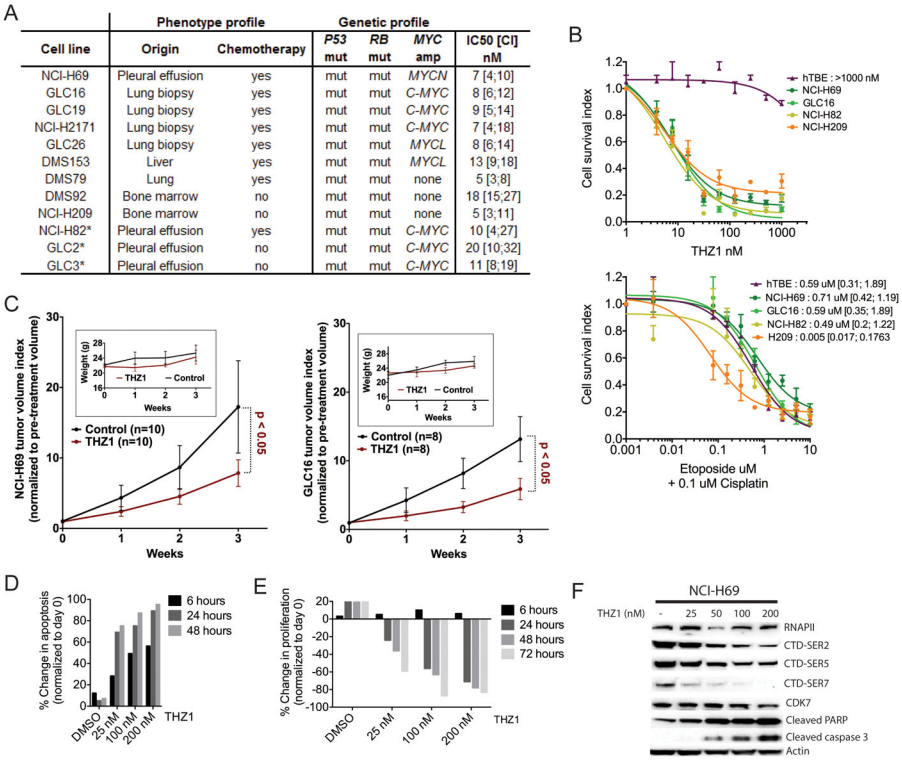

Figure 3. THZ1 is a potent inhibitor of cell viability and tumor growth in a panel of genotypic and phenotypic distinct SCLC cell lines and xenografts

A) Summary of THZ1 IC50s in the full panel of SCLC cell lines with genotype and phenotype status. IC50 data are presented as mean with confidence interval (mean [CI]). Phenotype profile information on cell lines comprises the following: origin - organ of origin of tissue specimen from which cell line was established; chemotherapy - whether patients had received chemotherapy before cell line establishment (yes/no). Genetic profile information on cell lines includes: *P53* and *RB* mutations (both leading to loss of function) and *MYC* gene family amplification (*C-MYC*, *MYCN* or *MYCL*). * indicates that cell lines have previously been classified as ‘variant’ neuroendocrine SCLC cell line based on the lack of expression of ‘classical’ neuroendocrine genes such as *ASCL1*, *NCAM*, *SCG2*.

B) Representative hSCLC cell lines (from A)) and the immortalized tracheobronchial epithelial (hTBE) cell line were exposed to increasing doses of THZ1 (top panel) or Cisplatin-Etoposide (lower panel) and IC50s were determined by cell viability assay. Each data point is shown as mean +/− SEM. Mean IC50s to Cisplatin-Etoposide treatment are reported next to cell line name (lower panel)

C) Tumor volume index of hSCLC xenografts grown on nude mice (NCI-H69: left panel; GLC16: right panel) as normalized to pre-treatment volume (day 0). Mice were treated with vehicle or THZ1. THZ1 was dosed at 10 mg/kg BID and vehicle BID. Inserts show weights from mice on treatment

D) Apoptosis assay measuring caspase 3/7 activity in the SCLC cell line NCI-H69 after THZ1 treatment for indicated time points.

E) Proliferation assay measuring BRDU incorporation in SCLC cell line NCI-H69 after THZ1 treatment for indicated time points.

F) Western blot detecting RNAPII, CTD phosphorylation (SER-2, SER-5, SER-7), and CDK7 along with the apoptotic markers Caspase 3 and PARP in total protein lysates from NCI-H69 cell lines exposed to indicated doses of THZ1. ACTIN serves as a loading control. See also Figure S3.

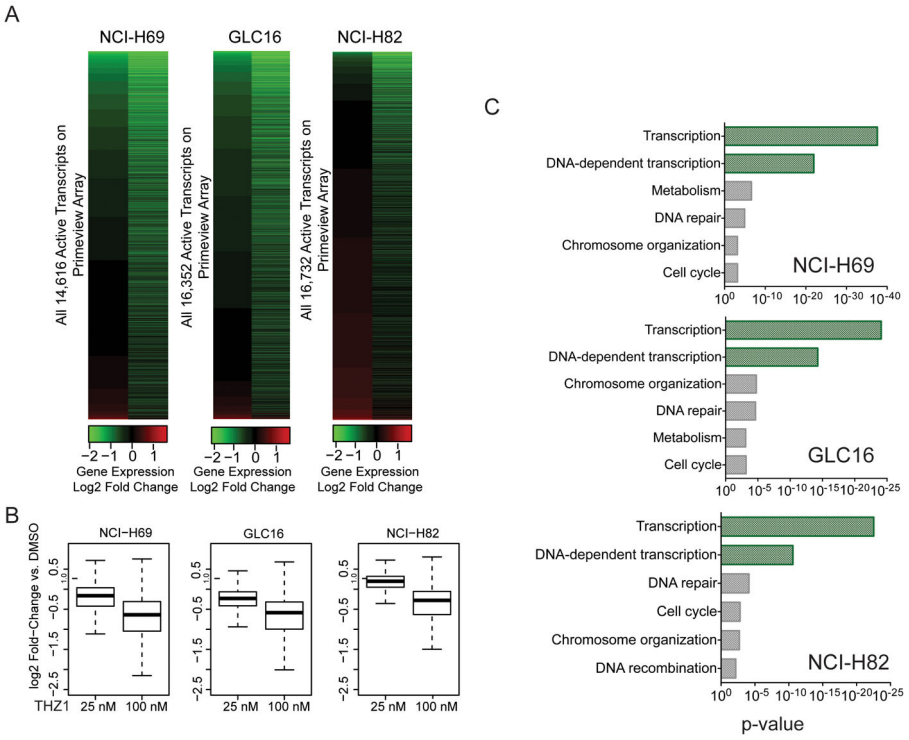

Figure 4. THZ1 treatment preferentially targets transcription-regulating genes in SCLC cells

A) Heatmap displaying the Log2 fold-change in gene expression versus DMSO for all active transcripts in NCI-H69, GLC16 and NCI-H82 cells following treatment with 25 nM and 100 nM THZ1 for 6 hours.

B) Box plots of Log2 fold-change in gene expression versus DMSO for all active transcripts in NCI-H69, GLC16 and NCI-H82 cells following treatment with 25 nM or 100 nM THZ1 for 6 hours. Whiskers extend to 1.5x the interquartile range.

C) Enrichment p-values for selected Gene ontology (GO) functional categories of top-5% downregulated genes (vs DMSO) of all active transcripts in NCI-H69, GLC16 and NCI-H82 cells following treatment with 100 nM THZ1 using DAVID software.

See also Table S1, Table S2, Figure S4.

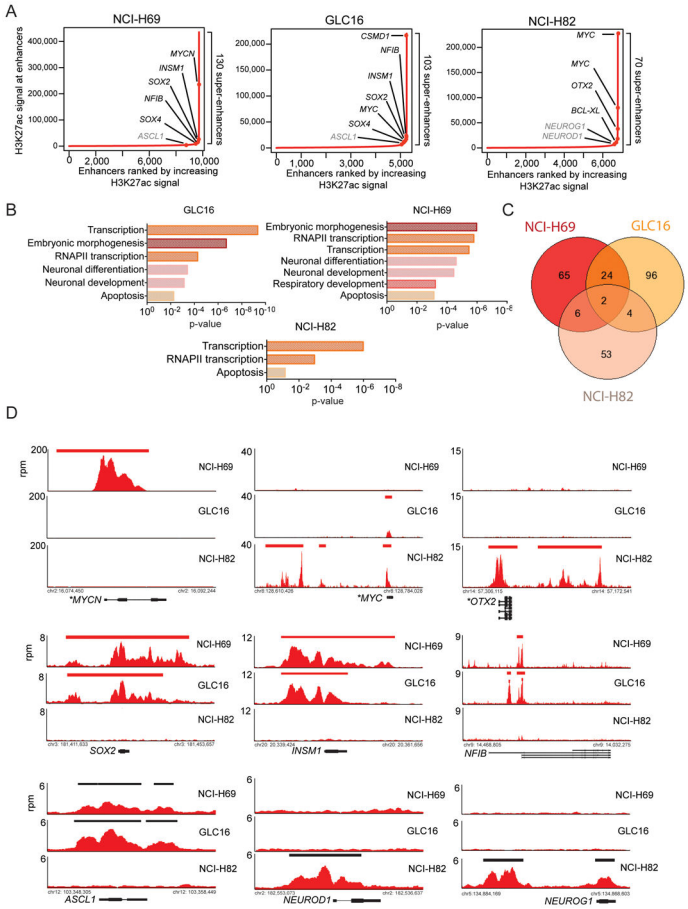

Figure 5. Super-enhancers in hSCLC cell lines are associated with proto-oncogenic and lineage-specific transcription factor genes

A) Distribution of H3K27Ac signal at enhancers. Enhancer regions are plotted in increasing order based on their input-normalized H3K27Ac signal (length*density) in NCI-H69, GLC16 and NCI-H82 cell lines.

B) Enrichment p-values for selected Gene Ontology (GO) functional categories of super-enhancer-associated genes in NCI-H69, GLC16 and NCI-H82 cell lines using DAVID.

C) Venn diagram showing overlap between identified super-enhancer genes between NCI-H69, GLC16, and NCI-H82 cell lines.

D) Gene tracks of H3K27Ac ChIP-seq occupancy and super-enhancer associated (top 2 rows) and typical-enhancer associated (bottom row) gene loci. The x-axis shows genomic position and the y-axis shows the signal of binding in 50bp bins in units of reads per million bin (rpm/bin). For genes with known focal amplification (*MYCN* (NCI-H69), *MYC* (NCI-H82, GLC16), input DNA signal-subtracted H3K27Ac signal is displayed (See Supplemental Experimental Procedures). Gene models are depicted below each track set. See also Table S3, Figure S5.

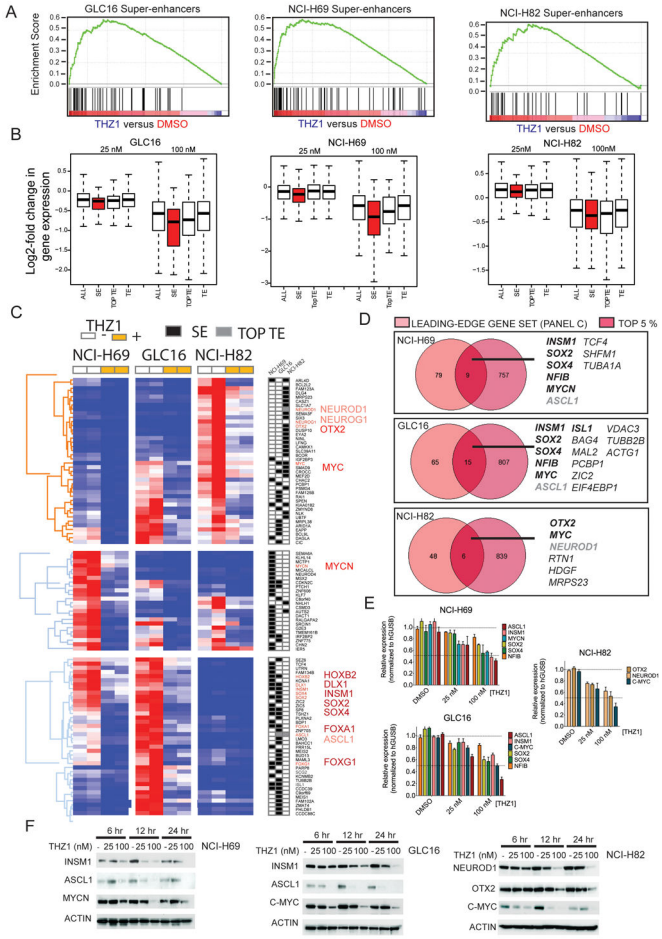

Figure 6. Identification of Super-enhancer-associated genes highly sensitive to THZ1 in SCLC cells

A) Gene set enrichment analysis (GSEA) plot showing significant enrichment of super-enhancer associated gene signature in 100 nM nM THZ1-treated cells relative to DMSO-treated cells.

B) Box plots of $\log_2$ fold-changes in mean transcript abundance of genes associated with the total pool of all enhancers (ALL), typical enhancers (TE), top ranked (largest) typical enhancers (TOPTE) and super-enhancers (SE) upon treatment with 25 or 100 nM THZ1 compared to control (DMSO). Whiskers extend to 1.5x the interquartile range.

C) Leading-edge genes identified from enrichment analysis in A) and corresponding heatmap of expression 'leading-edge genes' in DMSO- and 25 nM and 100 nM THZ1-treated cells.

D) Venn diagram showing overlap of 'leading-edge gene' sets as identified in (A) with the top-5% highest-expressed genes for each cell line. Gene names in black ***bold italics*** are transcription factors, and gene names in black *italics* are not transcription factors. Gene names in gray ***bold italics*** are transcription factors associated with a TOPTE.

E) Quantitative PCR to detect expression of indicated gene transcripts in DMSO, 25 nM and 100 nM THZ1-treated SCLC cells. Target gene expression is normalized to *GUSB*

expression and ‘DMSO’ serve as reference sample set to ‘Relative expression’ index 1). Data are presented as mean +/− SEM.

F) Western blotting to detect protein expression of indicated protein in DMSO, 25 nM and 100 nM THZ1-treated SCLC cells. ACTIN serves as a loading control.

See also Table S4, Figure S6.